Single Bunch Longitudinal Measurements at the Cornell Electron-Positron Storage Ring

R. Holtzapple, M. Billing, D. Hartill, and M. Stedinger
Laboratory of Nuclear Studies, Cornell University, Ithaca, NY 14853

B. Podobedov
Stanford Linear Accelerator Center, Stanford University, Stanford, CA 94309

Abstract

Measurements of the beam's bunch length in the Cornell Electron-Positron Storage Ring (CESR) have been made using a streak camera. The streak camera uses visible synchrotron radiation produced by the beam to measure its longitudinal distribution. A description of CESR, the experimental set up, the streak camera used, and systematic errors and analysis techniques of the streak camera are described in this paper. The dependence of the bunch distribution on the current and accelerating RF voltage for a single bunch in CESR was measured and compared with a theoretical model of CESR. The CESR vacuum chamber impedance is determined from the measured bunch distributions and is presented in this paper.

Introduction to CESR

In CESR, electrons collide with positrons at center of mass energies between 9.4-11.2 GeV. The accelerator complex is shown in figure 1. The main components of the accelerator complex are: 1) the electron gun which produces the electrons, 2) the linac which accelerates the electrons to 300 MeV to be injected into the synchrotron or is used to make positrons, 3) the synchrotron which accelerates the electrons and positrons to their final energy where they are injected by the transfer lines into CESR and 4) CESR. In CESR, four 5 cell RF cavities are used (for these measurements) to replace the energy lost due to synchrotron radiation. The new superconducting cavity had not been installed when the measurements were made. The energy of each beam can range between 4.7-5.6 GeV but normally CESR is either at 5.289 GeV or at 5.269 GeV depending on the requirements for high energy physics data. The measurements were performed at both energies and the difference in bunch length for these two different energies is negligible. CESR has a 768.43 meter circumference and the period of revolution is 2.56 μsec. Under normal colliding beam conditions at the time of the measurements there were nearly 9 evenly spaced bunch trains with two bunches in each train for a total of eighteen electron and eighteen positron bunches. Vertical and horizontal electrostatic separators are used to make a pretzel orbit to ensure separation between bunch crossings at locations other than the interaction region. During electron single bunch measurements the beam is in a pretzel orbit and for positron single bunch measurements the beam is in a flat orbit. CESR also has two wiggler magnets, located near the interaction region, which produce synchrotron radiation for the Cornell High Energy Synchrotron

Source (CHESS). Opening and closing the wiggler magnets affect the longitudinal phase space of the beam as will be discussed later.

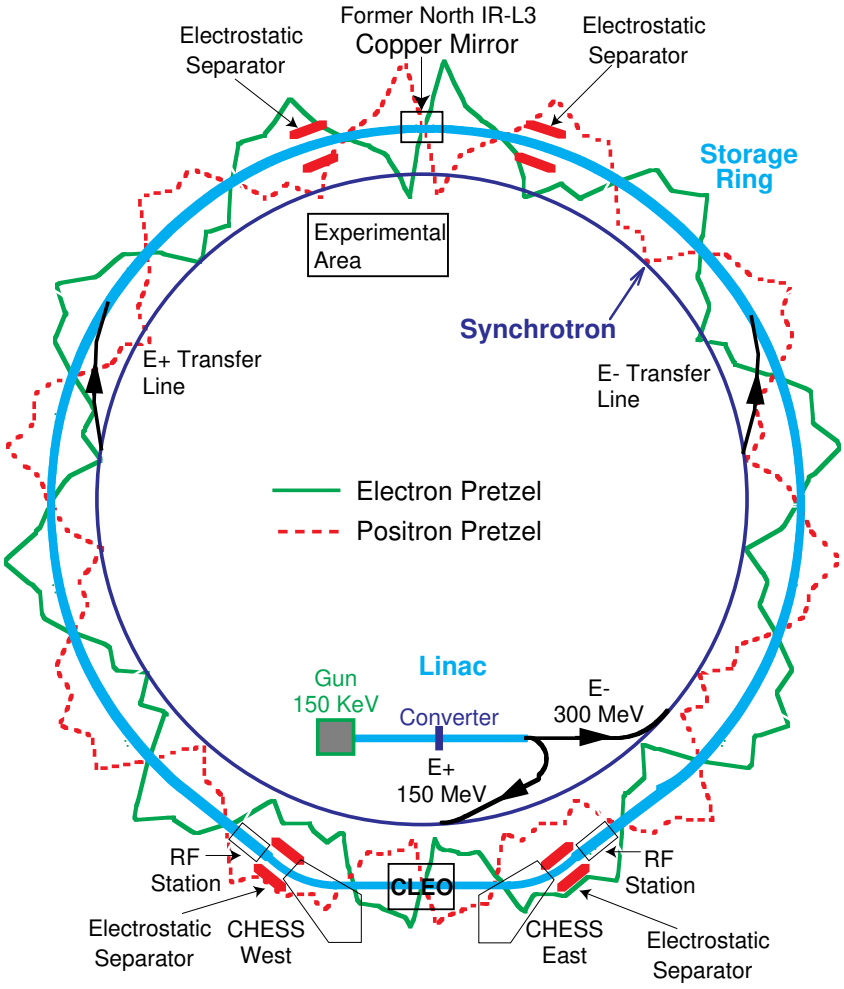

Figure 1. The layout of the Cornell Accelerator Complex. The streak camera experimental area and the mirror used to reflect the light out of the CESR vacuum chamber is located near the former North interaction region (IR).

Energy (on/off resonance)	5.289/5.269 GeV
Circumference	768.428 m
Revolution Period	2.563 μsec
RF Frequency	499.765 MHz
Horizontal Tune Qx	10.53
Vertical Tune Qy	9.61
Longitudinal Tune Qs	0.051
Harmonic number	1281

Table 1. Parameters of the CESR storage ring.

The measurements presented in this paper were taken when only one electron or positron bunch was present in CESR. The measurements were performed on both the electron and positron bunches when the opportunity for beam time was available. Some of the parameters of CESR are shown in Table 1.

Earlier measurements of the CESR bunch length, using a x-ray sensitive photoconducting detector and the beam spectrum, as a function of current have shown no bunch lengthening[10,11]. The resolutions of these previous measurements were not capable of measuring the effects presented in this paper.

CESR Single Bunch Dynamics

The longitudinal phase space in the storage ring is determined from accelerator components as well as from collective effects. In CESR, the electromagnetic fields which affect the bunch distribution are from the more than four hundred magnets which guide the bunches around the accelerator, two RF accelerating stations to counteract the bunch energy loss due to synchrotron radiation, and two wiggler magnets used to create synchrotron radiation for CHESS. The longitudinal phase space, ignoring collective effects, in a storage ring is Gaussian in both energy and length and has a phase space distribution given by [1]

$$\Psi(\tau,\varepsilon) = \exp\left[-\frac{\varepsilon^2}{2\sigma_\varepsilon^2} - \frac{\tau^2}{2\sigma_\tau^2}\right] \qquad (1)$$

where ε and τ are the energy and time deviation from a synchronous particle, σ_τ and σ_ε are the standard deviation of the bunch length and energy. The standard deviation bunch length is given by

$$\sigma_\tau = \left\langle \tau^2 \right\rangle^{1/2} = T_0 \sqrt{\frac{\alpha E_0}{2\pi h e V_{rf} \sin\phi_s}} \left(\frac{\sigma_\varepsilon}{E_0}\right) = \frac{\alpha}{\Omega_s} \sqrt{C_q E^2 \left(\frac{I_3}{2I_2 + I_4}\right)} \qquad (2)$$

where I_2, I_3, and I_4 are the synchrotron integrals. The term α is the momentum compaction, ω_{rev} and ω_{RF} are the revolution and RF frequencies, respectively, E_0 is the nominal energy, $h = \frac{\omega_{RF}}{\omega_{rev}}$ is the harmonic number, $\phi_s = \cos^{-1}\left(\frac{U_0}{eV_{RF}}\right)$ is the synchronous phase, V_{rf} is the RF accelerating voltage, and U_0 is the energy loss per turn for a synchronous particle. The synchrotron integrals, $I_1 - I_4$, in their integral and summations form are given by

$$I_1 = \oint\left(\frac{\eta}{\rho(s)}\right)ds = \sum_i \frac{l_i}{\rho_i}\langle\eta\rangle_i \qquad I_2 = \oint\left(\frac{1}{\rho^2(s)}\right)ds = \sum_i \frac{l_i}{\rho_i^2}$$

$$I_3 = \oint \left| \frac{1}{\rho(s)} \right|^3 ds = \sum_i \frac{l_i}{|\rho_i|^3}$$

$$I_4 = \oint \frac{(1+2k(s))\eta}{\rho^3(s)} ds = \sum_i \left[\frac{l_i}{\rho_i^3} \langle \eta \rangle_i + 2 l_i \left\langle \frac{K\eta}{\rho^3} \right\rangle_i \right]$$

where $\frac{1}{\rho(s)} = \frac{ecB(s)}{E}$ is the inverse of the radius of curvature for a dipole magnet, $\eta(s)$ is the dispersion, and $K(s) = \frac{ec}{E}\left(\frac{\partial B}{\partial x}\right)$ is proportional to the gradient of the field. The energy lost per turn, U_0, is also derived from the synchrotron integrals and is given by

$$U_0 = \frac{2}{3} r_e \frac{E_0^4}{\left(mc^2\right)^3} I_2 .$$

The synchrotron integrals can be determined for the CESR ring by knowing the length and radius of curvature of the dipole magnets (table 2), the dispersion, gradient of the fields, and wiggler magnet parameters. The synchrotron integrals that reflect CESR when the streak camera experiments were performed are denoted in table 3.

Number of Magnets	Magnet Length L(m)	Radius of Curvature ρ(m)
4	6.572	58.603
62	6.573	87.891
4	2.945	140.626
8	3.236	31.654
2	1.644	87.892
2	3.287	87.892
2	3.176	34.818

Table 2. The magnet length and radius of curvature for the 84 dipole magnets in CESR.

The energy spread of CESR is dependent on the energy and bending radius. The energy fluctuations depend on the bending radius and do not change as the bunch distribution changes, so the bunch remains Gaussian in energy. The energy spread can be determined from the synchrotron integrals to give

$$\left(\frac{\sigma_\varepsilon}{E}\right) = \sqrt{\frac{C_q \gamma^2 I_3}{2I_2 + I_4}} \qquad (3)$$

where the constant $C_q = 3.84 x 10^{-13} m$. Measuring the energy spread in a storage ring to a high degree of accuracy is a difficult task. Ideally making measurements with a high resolution camera or wire scanner located in a high dispersion region is the preferred method to measure the energy spread.

Presently the only energy spread measurement on CESR was done by the CLEO detector on the 1s and 2s resonance. The result of these measurements is that the energy spread on the 1s and 2s resonance is consistent with being constant as a function of current.

	Wigglers Open	Wigglers Closed
I_1	$8.791m$	$8.791m$
I_2	$9.336x10^{-2}\,m^{-1}$	$1.047x10^{-1}\,m^{-1}$
I_3	$1.716x10^{-3}\,m^{-2}$	$2.372x10^{-3}\,m^{-2}$
I_4	$2.088x10^{-3}\,m^{-1}$	$2.744x10^{-3}\,m^{-1}$
I_5	$3.890x10^{-4}\,m^{-1}$	$5.386x10^{-4}\,m^{-1}$
U_0	$1.0290MeV$	$1.1541MeV$
$\frac{\sigma_E}{E}$	$6.115x10^{-4}$	$6.782x10^{-4}$
σ_Z	$1.565x10^{-2}\,m$	$1.739x10^{-2}\,m$

Table 3. The synchrotron integral for CESR for the case when the wiggler magnets are open (CHESS is not collecting data) or closed.

It should be noted that the energy spread and bunch length from equations 2 and 3 are their equilibrium values at low currents. The relationship between σ_τ and σ_E/E_0 depends on the local slope of the RF waveform and beam induced fields can distort the bunch shape even while the energy spread remains Gaussian. As the intensity of the bunch increases, collective effects that modify the slope of the RF wave, have to be included. In CESR there are several phenomena that affect the single bunch distribution and they are:

1. Beam Induced Voltage-Potential Well Distortion

For single particle motion, the bunch distribution in equilibrium has a Gaussian distribution and the length depends upon the RF accelerating voltage. In the same manner that the RF accelerating fields affect the bunch distribution, beam induced voltages from longitudinal wakefields also influence the shape of the bunch distribution. The beam induced voltages are categorized into three different types and their influence on the longitudinal dynamics of CESR will be examined.

The beam induced voltages described in this section result in potential well distortion of the bunch distribution. With potential well distortion, the bunch distribution is static but distorted from a Gaussian distribution by the beam induced voltage[3]. We observe in CESR a greater distortion for higher beam intensity. There is another possibility, which is that the distribution is not static but instead performs a collective oscillation. This is discussed later.

The steady state distribution can be determined by solving the Vlasov equation where $\psi(\varepsilon,\tau)$ is the phase space distribution normalized to unity[4,5]. The Vlasov equation is used to describe a multiparticle system that is influenced by electromagnetic fields. In our case, the Vlasov equation is

$$\frac{\partial\psi}{\partial t}+\dot{\tau}\frac{\partial\psi}{\partial\tau}+\dot{\varepsilon}\frac{\partial\psi}{\partial\varepsilon}=0$$

where

$$\dot{\tau}=-\alpha\frac{\varepsilon}{E_0}$$

and

$$\dot{\varepsilon}=e\frac{V(\tau)-U(\varepsilon)}{T_0}\cdot$$

The longitudinal phase space can be modified to include the beam induced voltage terms. Now the term $V(\tau)$ includes the RF accelerating voltage and the beam induced voltage. The induced voltage can be expressed in terms of three different categories; one which has time dependence identical to the input current (resistive part), the second which has time dependence like the derivative of the input current (inductive part), and the third which has time dependence like the integral of the input current (capacitive part). Including the above terms, the function $V(\tau)$ can be written as[4]

$$V(\tau)=V_{rf}(\tau)+V_b(\tau)=V_{rf}\cos(\omega\tau+\varphi)+RI_b(\tau)+L\frac{dI_b(\tau)}{d\tau}+\frac{1}{C}\int_{-\infty}^{\tau}d\tau' I_b(\tau') \quad (4)$$

where $V_{rf}(\tau)$ is the RF accelerating voltage and the three other terms are the induced voltages from the resistive (R), capacitive (C), and inductive (L) impedance of the CESR vacuum chamber. The bunch shape is a function of the resistance, capacitance, and inductance. The beam current, $I_b(\tau)$, is given by

$$I_b(\tau)=Ne\int_{-\infty}^{\infty}d\varepsilon\psi(\varepsilon,\tau)$$

where N is the total number of particles in the bunch and the phase space distribution is normalized to unity which requires that

$$\int_{-\infty}^{\infty}d\tau d\varepsilon\psi(\varepsilon,\tau)=1\cdot$$

Vlasov's equation can now be expressed as

$$\frac{\partial\psi}{\partial t}-\alpha\frac{\varepsilon}{E_0}\frac{\partial\psi}{\partial\tau}+\frac{eV(\tau)-U(\varepsilon)}{T_0}\frac{\partial\psi}{\partial\varepsilon}=0$$

To calculate the steady state bunch distribution, the distribution function $\psi(\varepsilon,\tau)$ is time independent ($\frac{d\psi}{dt}=0$). To study the potential well distortion we will require the following simplifying assumptions:

1) The energy loss per turn is constant ($U(\varepsilon)=U_0$).
2) The energy spread remains constant at σ_ε.

From these assumptions we find that the energy and time variables are independent. Now the energy and time dependence can be written separately as

$$\psi(\tau,\varepsilon)=\rho(\tau)\phi(\varepsilon)$$

which results in the two equations, one for the energy deviation

$$\phi(\varepsilon)=\frac{\sigma_\varepsilon}{\sqrt{2\pi}}\exp\left(\frac{-\varepsilon^2}{2\sigma_\varepsilon^2}\right)$$

and for the time deviation

$$\frac{\partial\rho}{\partial\tau}=\frac{-E_0}{\sigma_\varepsilon^2}\left[\frac{eV(\tau)-U_0}{\alpha T_0}\right]\rho(\tau) \qquad (5)$$

There are two points that can be made about the two above equations:

1) The distribution is Gaussian in the energy deviation ε and as the current increases the distribution remains Gaussian in ε, the distribution in time does not have to remain Gaussian in τ.
2) At low current and with $\omega\tau << 1$, the beam induced voltage $V_b(\tau)\approx 0$, which results in the distribution being Gaussian in τ and expressed as

$$\rho(\tau)=\frac{\sigma_\tau}{\sqrt{2\pi}}\exp\left(\frac{-\tau^2}{2\sigma_\tau^2}\right)$$

The expression for the beam induced voltage (equation 4) can be substituted into equation (5) and the resulting expression for the charge distribution is written as [4]

$$\frac{\partial\rho(\tau)}{\partial\tau}=\frac{-eE_0\rho(\tau)}{\sigma_\varepsilon^2\alpha T_0}\left[\frac{V_{rf}\cos(\omega\tau+\varphi)+QR\rho(\tau)+\frac{Q}{C}\int_{-\infty}^{\tau}d\tau'\rho(\tau')-U_0}{1+\frac{eE_0QL\rho(\tau)}{\sigma_E^2\alpha T_0}}\right] \qquad (6)$$

where Q is the total charge in the bunch. The charge distribution, $\rho(\tau)$, can be determined numerically by integrating equation 6. The general formalism for calculating the distribution of particles in CESR using Vlasov's Theory is described elsewhere[4]. The simulations presented here are an updated version of the software developed earlier that numerically integrates equation 6 to determine the bunch distribution for the given input parameters. The following are three examples of the bunch distribution determined by numerically integrating equation 6 with the CESR parameters listed in table 4.

E_0	5.289 GeV
σ_ε / E_0	6.782×10^{-4}
T_0	2.56×10^{-6} sec
α	1.14×10^{-2}
V_{rf}	6.87 MV
U_0	1.15 MeV

Table 4. The parameters used in the numerical analysis to determine the CESR bunch distribution. The parameters listed here are representative of the CESR beam when the wiggler magnets are closed.

(i) Resistive Impedance Beam Induced Voltage

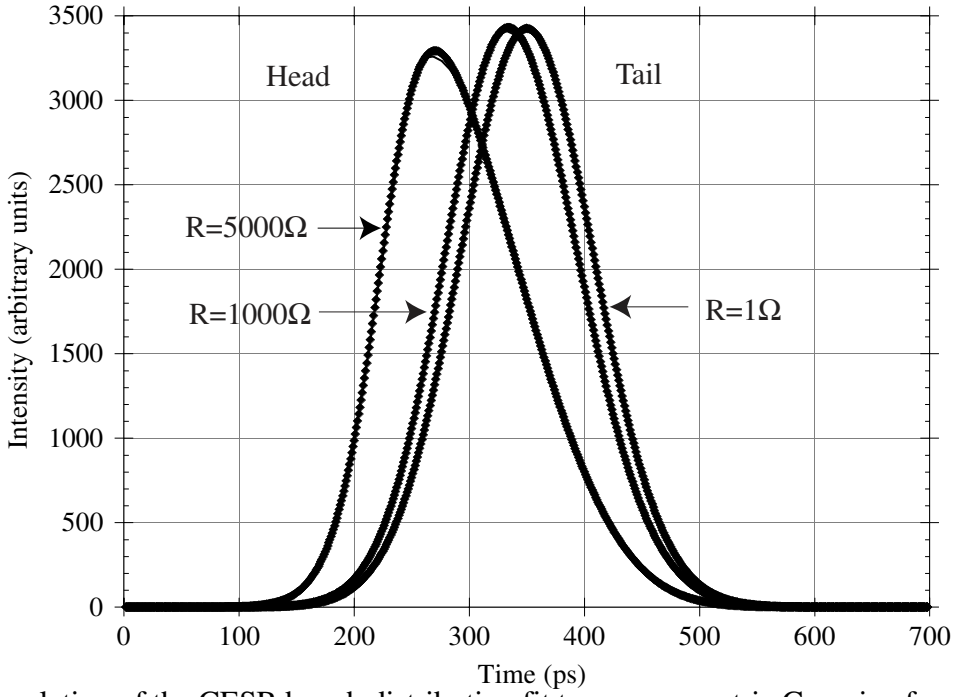

Figure 2. A simulation of the CESR bunch distribution fit to an asymmetric Gaussian function at several different resistance values. The single bunch current for this simulation is 20 mA and the CESR machine parameters used to determine the bunch distribution are listed in table 4.

When the slope of the beam induced voltage is in phase with the RF accelerating voltage it is considered a resistive beam induced voltage, and as a result, the bunch distribution becomes asymmetric in shape. The vacuum elements in CESR that give rise to resistive beam induced voltage are the RF and other large cavities. A pure resistive beam induced voltage is proportional to the charge density and is given by

$$V_b(\tau) = RI(\tau)$$

where R is the resistance and I is the bunch current. The charge distribution for a resistive beam induced voltage can be numerically integrated (ignoring the capacitive and inductive terms) from

equation 6. Figure 2 is an example of the CESR bunch distribution at a fixed current for several different resistance values. As the resistance is increased the bunch tilts, becoming more asymmetric in shape, to compensate for the increased higher order mode loss.

The simulated bunch distributions are fit to an asymmetric Gaussian function (described later in this paper) in order to quantify the change in the length and asymmetry of the distribution. The bunch length and asymmetry factor as a function of current and resistance is plotted in figures 3 (a) and (b). The bunch length does increase as a function of current for a fixed resistance.

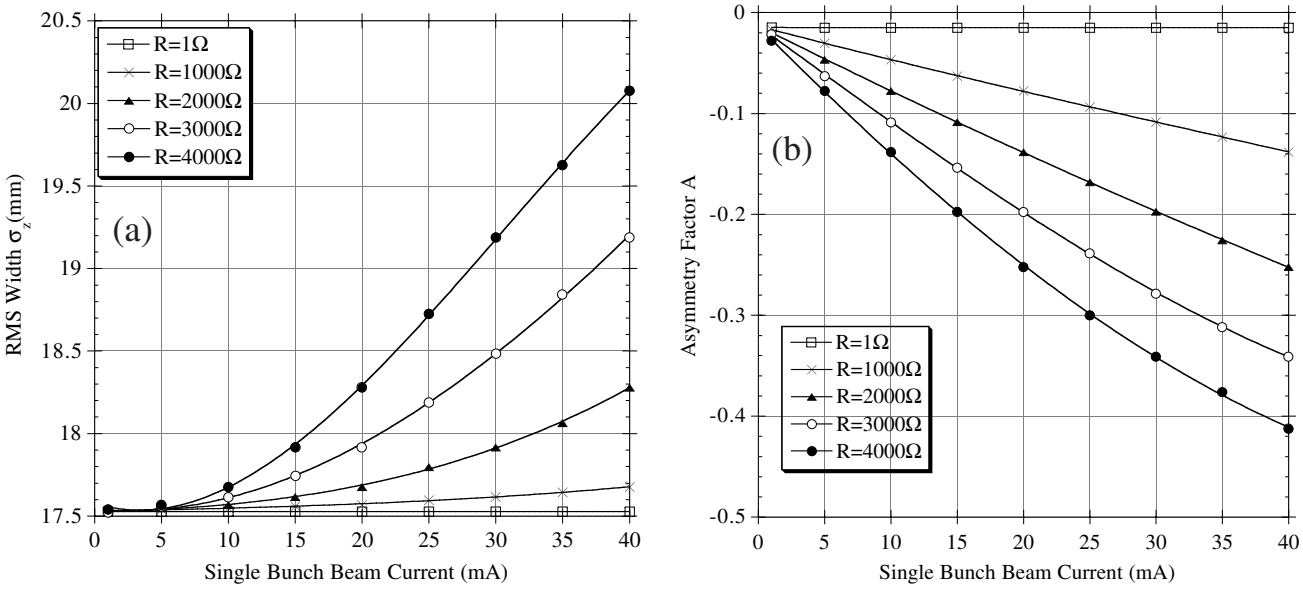

Figure 3. Results of the simulation of the CESR (a) bunch length and (b) asymmetry factor as a function of current at several different resistance values.

The resistive impedance of the CESR vacuum chamber has been measured by two different methods: (i) measuring the higher order mode loss and (ii) measuring the bunch distribution. The higher order mode loss factor, k_{HOM}, was measured on CESR to be [6]

$$k_{\substack{HOM \\ open}} = 7.53 \pm 1.13 \ \frac{\mathrm{V}}{\mathrm{pC}} \text{ and } k_{\substack{HOM \\ closed}} = 6.64 \pm 1.00 \ \frac{\mathrm{V}}{\mathrm{pC}}$$

with the wiggler magnets open and closed respectively. This results in a resistive impedance of

$$R_{open} = 1393 \pm 209 \ \Omega \text{ and } R_{closed} = 1365 \pm 205 \ \Omega$$

with the wiggler magnets open and closed respectively. Using the bunch distribution measurements by the streak camera, the resistive impedance can also be determined and is presented in the analysis section of this paper.

(ii) Inductive Impedance Beam Induced Voltage

When the beam induced voltage opposes the slope of the RF accelerating voltage then it is considered to be inductive and as a result bunch lengthening occurs. If the impedance is modeled as pure inductance, the beam induced voltage is proportional to the derivative of the charge density and is expressed as

$$V_b(\tau) = L\frac{dI}{d\tau}$$

where L is the inductance. The vacuum components in a storage ring that cause inductive induced voltages are masks, bellows, and abrupt transitions in vacuum chamber. Figure 4 is an example of the numerically integrating equation 6 for the CESR bunch distribution at a fixed current for several different values of the inductance. Notice that as the inductance is increased the peak of the distribution becomes flatter and it remains symmetric around the origin. This symmetry is a result of no energy loss from a perfect inductive induced voltage.

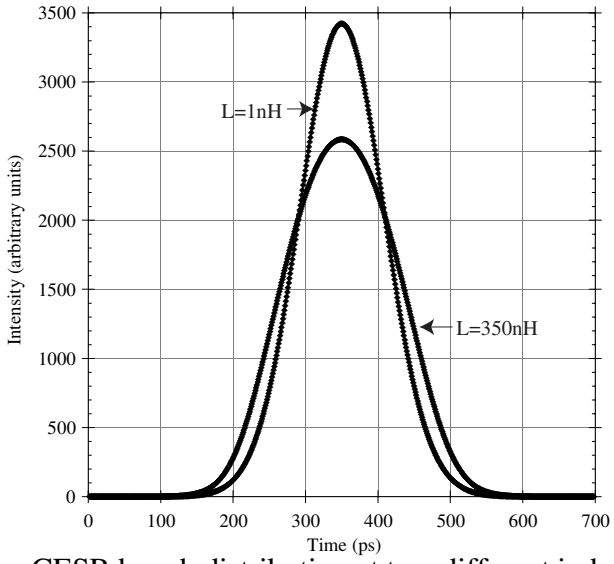

Figure 4. A simulation of the CESR bunch distribution at two different inductance values. The parameters used to determine the bunch distribution are listed in table 4 and the bunch current is 20 mA. The bunch distributions are not fit to a function but instead the full width at half maximum of the bunch is used to characterize the bunch length.

As the inductance increases the bunch shape deviates from a Gaussian distribution. The bunch length is determined by calculating the full width half maximum (FWHM) divided by 2.355. Figure 5 is the simulated bunch length as a function of current for several different inductance values. The bunch length increases as a function of current for a fixed inductance. In CESR, the bunch shape is fairly Gaussian at low current and becomes asymmetric, due to the resistive impedance, as the current is increased.

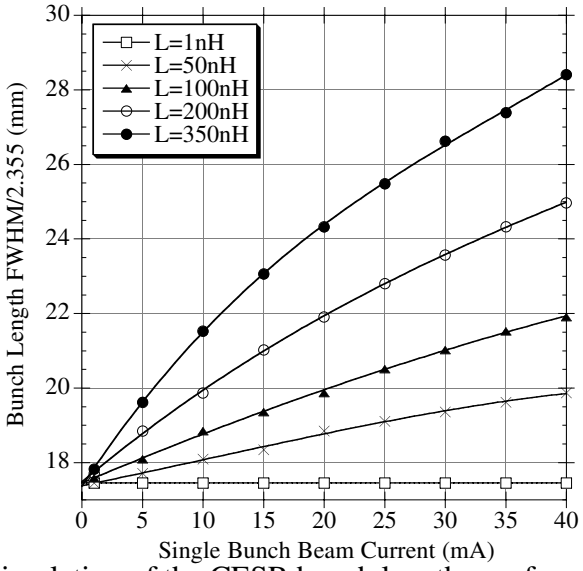

Figure 5. The results of the simulation of the CESR bunch length as a function of current at several different inductance values.

(iii) Capacitive Impedance Beam Induced Voltage

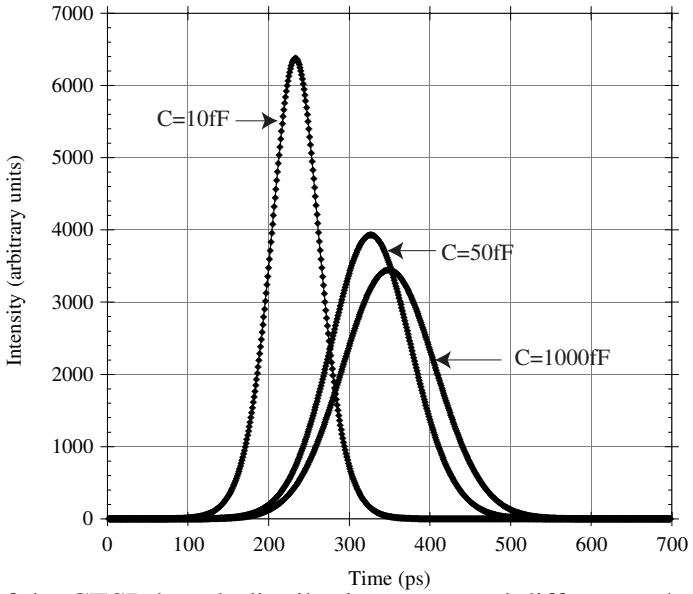

Figure 6. A simulation of the CESR bunch distribution at several different values of the capacitance. The parameters used to determine the bunch distribution are listed in table 4 and the current of the bunch for the simulations is 20 mA.

When the beam induced voltage is proportional to the integral of the current then it is considered to be capacitive and as a result bunch shortening occurs. If the beam induced voltage is modeled as pure capacitive, the beam induced voltage is proportional to the integral of the derivative of the charge density and is expressed as

$$V_b(\tau) = \frac{1}{C}\int_{-\infty}^{\tau} d\tau' I_b(\tau')$$

where C is the capacitance, and I is the bunch current. The vacuum chamber components in a storage ring that cause capacitive induced voltages are RF and other deep cavities. Figure 6 is an example of the CESR bunch distribution, numerically integrated from equation 6, at a fixed current for several different capacitive values. As the inverse of the capacitance is increased the bunch is shortened and shifted due to the increase in voltage.

The bunch length for the simulated bunch distribution as a function of current and capacitance is determined by calculating the full width half maximum divided by 2.355 as is plotted in figure 7. The bunch length does decrease as a function of current for a fixed capacitance.

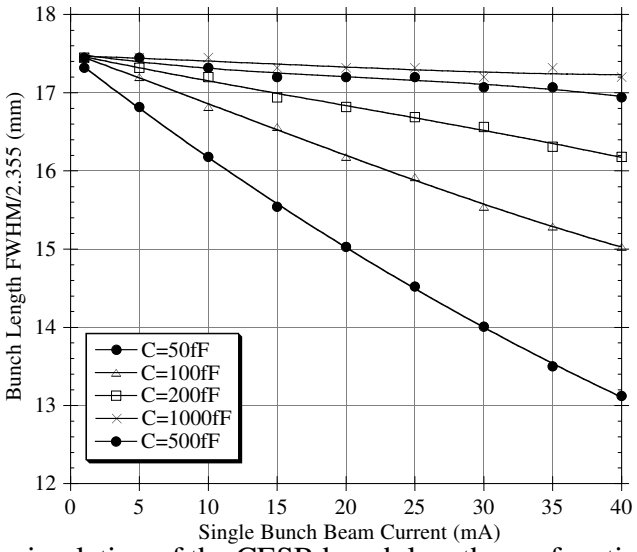

Figure 7. The results of the simulation of the CESR bunch length as a function of current at several different capacitive values. The bunch length is the FWHM of the distribution divided by 2.355.

The above examples illustrate how the beam induced voltage can change the bunch distribution in CESR. In reality, the impedance of the CESR vacuum chamber consists of resistive, inductive and capacitive parts. For the bunch lengths measured in CESR, the capacitive impedance has a small effect on the bunch length and can be ignored. In principle, the particle distributions measured in CESR can be used to measure the dominant components of the impedance that will be presented later.

2. Longitudinal Instabilities

The discussion above has assumed that a steady state of the beam exists and it is stable. This cannot be taken for granted when longitudinal wakefields are present. What usually happens is that the beam becomes unstable above some threshold current. The general methods of analysis of instabilities are to linearize Vlasov's equation for small perturbations or to use computer simulations. One result is that the energy spread no longer remains constant as it does with potential well distortion. An increase

in the energy spread is the signature of an instability and is a better method than measuring the bunch length for determining a current threshold for an instability. Due to our inability to measure the energy spread, the bunch length measurements will have to suffice.

There is an instability in CESR, but it is a multi-bunch effect and is not seen with a single bunch. Potential well distortion from beam induced voltage is the dominant effect with single bunch running.

Experimental Set-up

The streak camera uses synchrotron radiation produced by the accelerator dipole magnets to determine the longitudinal bunch distribution. When the bunch travels through the dipole magnet it emits a pulse of synchrotron light which contains the longitudinal distribution of the bunch. The electrons (or positrons) in the head of the bunch emit light before the electrons in the tail of the bunch and the longitudinal intensity of this pulse of light is proportional to the number of particles located longitudinally in the bunch. The light pulse has the longitudinal profile encoded in its length and the streak camera will decode this information. The synchrotron light pulse is transported from the source out of the vacuum chamber to a safe location shielded from radiation where the streak camera measurements can be made. The location in CESR where the measurements were performed is ideal because synchrotron light from both electrons and positrons can be observed from identical magnets for both beams and the same optics can be used to deliver the light to the streak camera. The dipole magnet and optics used to transport the light out of the CESR vacuum chamber is shown in figure 8.

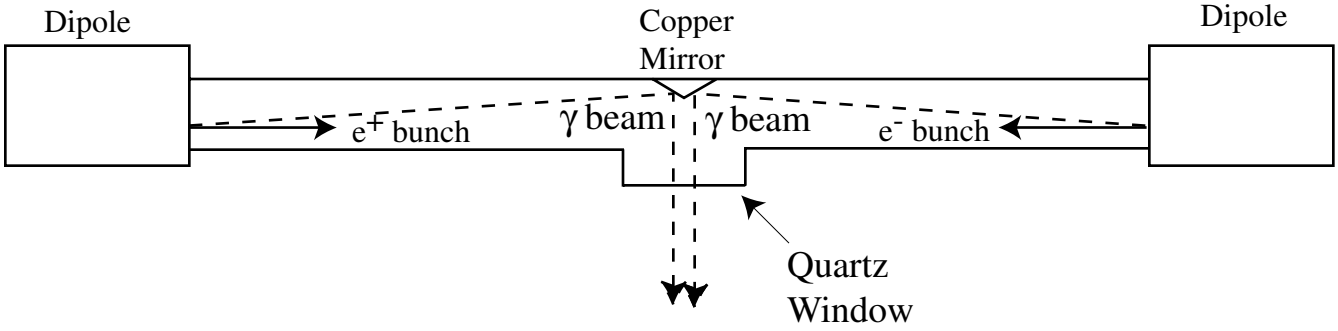

Figure 8. A cross sectional view looking vertically down on the vacuum chamber where the copper mirror is located in CESR. Synchrotron light from both beams is emitted in the dipole magnet and strikes the mirror that transports the light out of the vacuum chamber.

The synchrotron light is emitted by the beam traveling through a dipole magnet adjacent to the straight section in the old detector location called L3 (figure 1). The synchrotron light is reflected by a highly polished water cooled copper mirror which is cut at a 45 degree angle to the vacuum chamber wall, and the visible light passes through a quartz window out of the vacuum chamber. The copper mirror was polished by hand with a jig that holds the mirror at an angle of 45 degrees to a flat polishing wheel. Diamond polishing compound as fine as one micron was used to ensure the flatness and

reflectivity of the mirror. The mirror was designed to protrude into the vacuum chamber wall 1 centimeter. After the mirror the synchrotron light is then transported over the synchrotron and through a hole in the steel of the old detector. The light is transported by a series of 7 mirrors, which includes 2 periscopes, over a distance of approximately 56 ft from the light source to the location of the streak camera. The second mirror in the set up can be moved transversely by remote control to allow for tuning of either the electron or positron synchrotron light. There are three lenses used to focus the light on the streak camera slit. The first lens has a focal length of 1.5m and located just inside the radiation shielded experimental hall. The second lens is a cylindrical one, which spreads the light horizontally across the slit of the camera. The third lens is located approximately 3 inches from the camera and is used for additional focusing on the slit of the camera.

The properties of the dipole magnets which produce the synchrotron light is shown in table 5.

Length	2.9453 m
Pole Tip Field	1.25 kG
$\int \vec{B} \bullet d\vec{l}$	3.70 kG-m
Bend angle	20.944 mrad
Radius of Curvature	140.628 m
Synchrotron Radiation Opening Angle	0.0966 mrad
Synchrotron Radiation Critical Energy	2.33 KeV
Synchrotron Radiation Critical Wave length	0.511 nm

Table 5. The dipole magnet and synchrotron radiation parameters for the streak camera experiment. All the parameters are for an energy in CESR of 5.289 GeV.

Description of the Streak Camera[7]

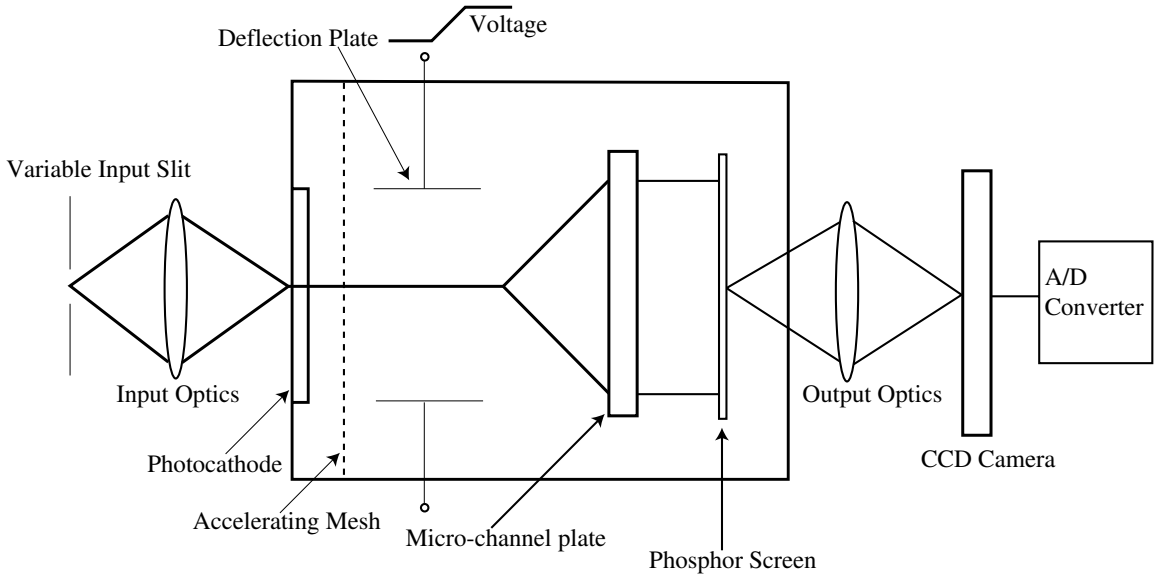

Figure 9. The layout of the Hamamatsu streak camera.

The streak camera is a device to measure ultra-fast pulsed light intensity versus time. The streak camera used in this experiment was a Hamamatsu model N3373-02 camera made by Hamamatsu Photonics. The basic components of the streak camera are shown in figure 9, and they are the variable input slit, input optics, photo cathode, accelerating mesh, deflection plate, micro-channel plate, phosphor screen, output optics, CCD camera, and analog to digital read-out system.

The streak camera measures the bunch distribution in the following manner. Consider a pulse of light that consists of four photons that are separated in time as they enter the streak camera (see figures 10 (a) and (b)). These four photons can be tracked through the camera to illustrate its basic operations.

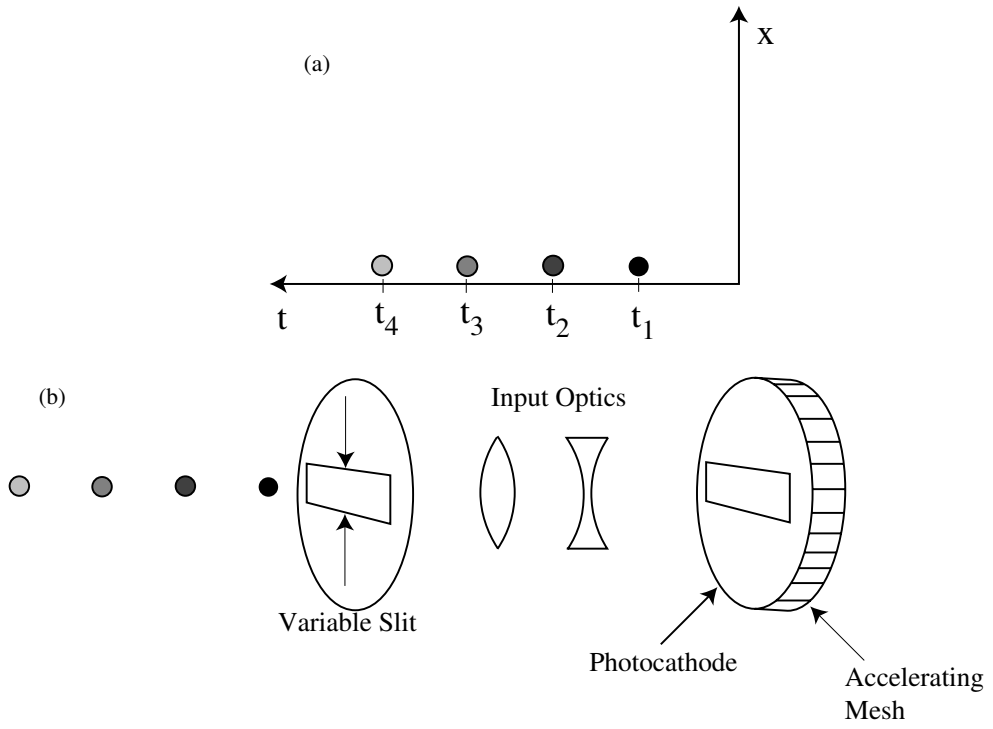

Figure 10. (a) The four photons that make up the pulse of light that enter the streak camera are separated in time. (b) The four photons entering the streak camera.

The four photons enter the streak camera through a variable vertical slit that is typically 200 μm wide. The photons are transported through the streak camera input optics. The input optics form an image of the variable slit onto a photocathode. The photons hit the photocathode of the streak tube where they are converted to photoelectrons. The number of photoelectrons produced is proportional to the number of the photons. The photoelectron pulses are again spaced by the arrival time of the photons. The emitted photoelectron pulses are accelerated by an accelerating mesh that pulls the photoelectrons away from the photocathode and keeps the pulses separated in time. The electrons pass between deflecting plates where a high voltage is applied at a time synchronized to the incident light (figure 11). The timing of the incident pulse initiates a very high speed sweep of the high voltage.

During the high speed sweep, the electrons are deflected at different angles depending upon their arrival time at the deflection plates. After deflection the electrons enter the micro-channel plate.

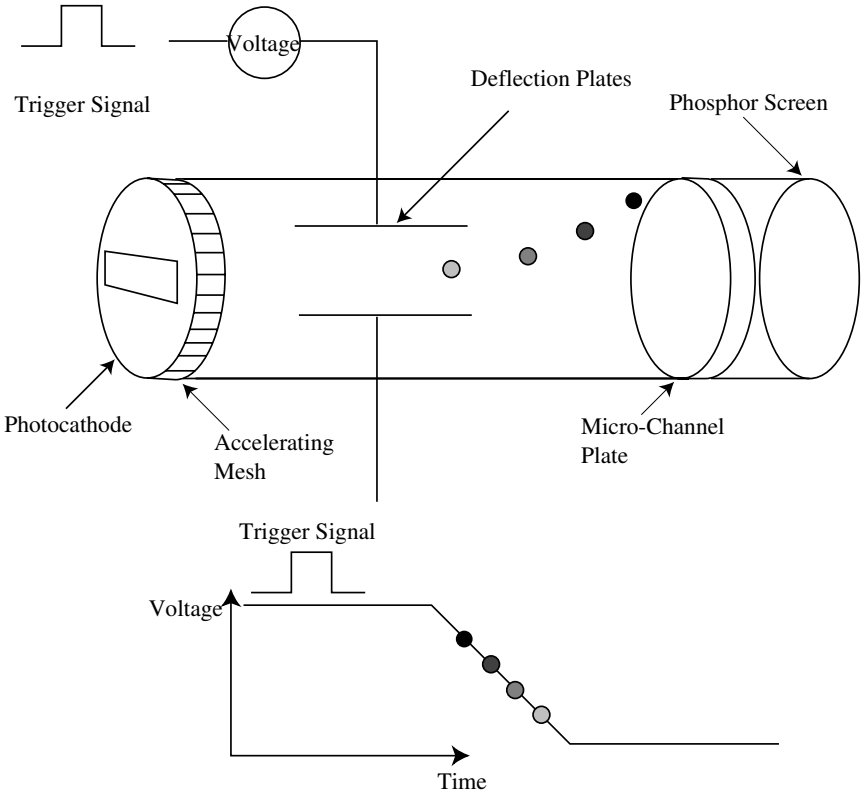

Figure 11. The trigger signal is synchronized with the arrival of the photoelectrons at the deflecting plate.

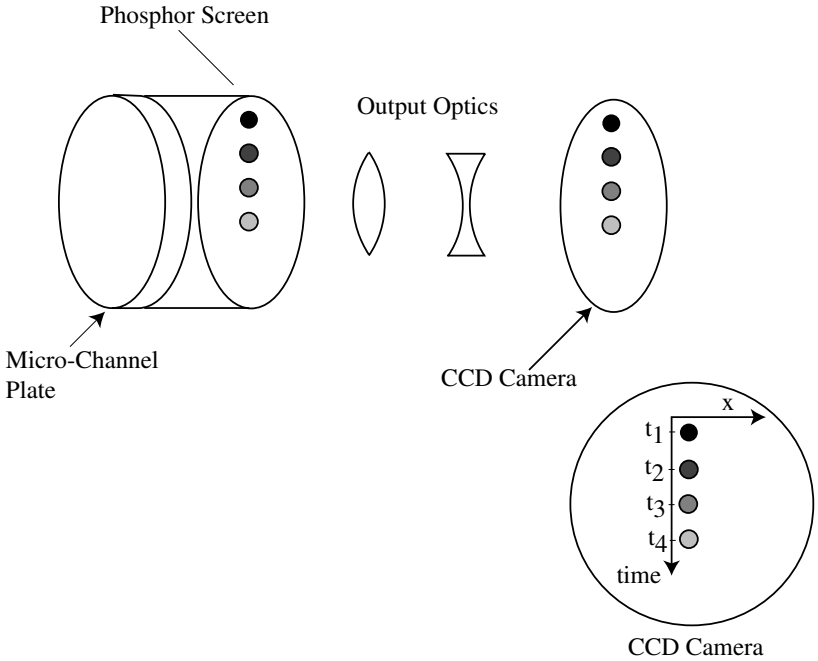

Figure 12. The output of the streak camera.

The micro-channel plate multiplies the electron pulse by several thousand times. After the micro-channel plate, the photoelectrons strike a phosphor screen where they are converted into light again. The brightness of the phosphor screen is proportional to the intensity of the pulse. The vertical axis on the phosphor screen is the time axis (figure 12). The image on the phosphor is transported by the output optics to a cooled CCD camera where the image is then digitized and processed by a computer.

The streak camera resolution is dependent on the streak speed of the camera and on the slit width used. This particular streak camera has four different streak speeds, 60 ps/10 mm, 200 ps/10 mm, 500 ps/10 mm and 1.2 ns/10 mm.

Method of Data Analysis

The streak camera takes images of the bunch distribution which are 512 by 512 pixels in size. A selected area can be chosen such that the vertical columns in that area are projected on the horizontal axis. This creates a profile that can be fit to a function that characterizes the distribution of the bunch.

The bunch distribution in CESR deviates from a pure Gaussian distribution due to potential well distortion. The function used to characterize the bunch shape is an asymmetric Gaussian function. The longitudinal profiles of the beam distribution are fitted to an asymmetric Gaussian function with a constant background given by

$$I(z) = I_0 + I_1 \exp\left\{-\frac{1}{2}\left(\frac{(z-\bar{z})}{(1+sgn(z-\bar{z})A)\sigma}\right)^2\right\}$$

where I_0=pedestal, I_1=peak of the asymmetric Gaussian. The term $sgn(z-\bar{z})A$ is the asymmetry factor that parameterized the shape of the asymmetric Gaussian. Figure 13 is a profile of the selected area with a fit to an asymmetric Gaussian function. The longitudinal profile of the beam distribution in CESR is χ^2 minimized using the minimization package Minuit[8]. A χ^2 minimization was performed on each streak camera picture

$$\chi^2 = \sum_i^n \frac{\left[I(z_i; A, I_0, I_1, \bar{z}, \sigma) - x_i\right]^2}{x_i}$$

where x_i is the digitized signal from the streak camera profile. The fit returns the mean $\bar{z}$, asymmetry factor A, background level I_0, peak of the asymmetric Gaussian I_1, and width σ of the distribution. The pertinent information retrieved from the asymmetric Gaussian function is the rms width

$$\sigma_z = \text{rms width} = \left\langle \left(z - \langle z \rangle\right)^2 \right\rangle^{1/2} = \left[1 + \left(3 - \frac{8}{\pi}\right)A^2\right]^{1/2} \sigma,$$

the mean of the distribution

$$\langle z \rangle = \text{mean} = \bar{z} + 2\sqrt{\frac{2}{\pi}} A\sigma$$

and the asymmetry factor A. These quantities are the quoted results from the measurements.

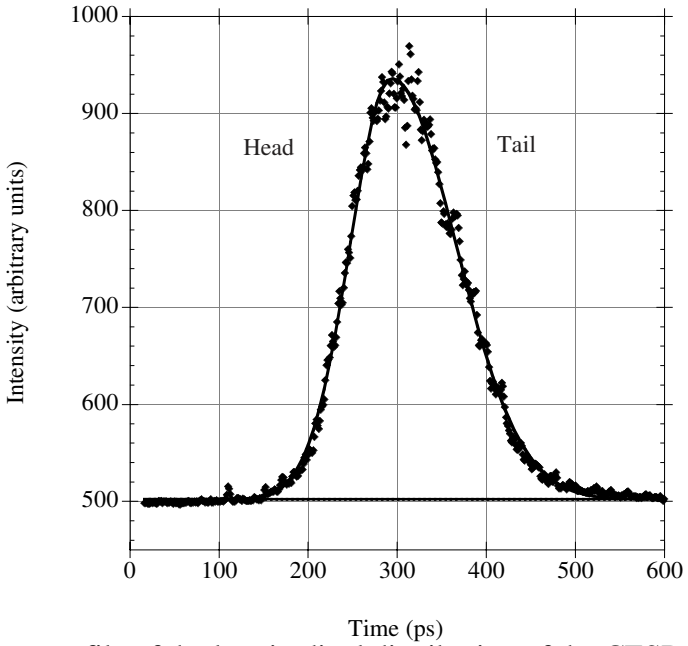

Figure 13. A streak camera profile of the longitudinal distribution of the CESR beam fit to an asymmetric Gaussian function. The head of the bunch (early in time) is to the left. This particular profile was taken with a single bunch current of 30.7 mA.

Many experiments were performed on CESR under different machine parameters. During each experiment a set of data, which consists of at least 10 streak camera pictures, was taken under the same accelerator conditions. The mean rms width, σ_z, and asymmetry factor, A, from each experiment was used to examine the pulse to pulse fluctuations in the beam distribution. Fitting each streak camera distribution to the mean rms width and asymmetry factor and letting the area and mean position of the asymmetric Gaussian function vary, the difference, or residual, between the fit and the data show variations between an average distribution and individual pictures. The residual, R_{ij}, is the jth pixel from the experiment with i streak camera profiles. The residual was determined from the expression

$$R_{ij} = x_j - I\left(z_j; \overline{A}, I_0, I_1, \bar{z}, \overline{\sigma}\right) \qquad (7)$$

where $I\left(z_j; \overline{A}, I_0, I_1, \bar{z}, \overline{\sigma}\right)$ is determined by doing a χ^2 fit to the asymmetric Gaussian function using the mean sigma ($\overline{\sigma}$) and mean asymmetry factor ($\overline{A}$) from the given experiment (these quantities are held constant in the fit), and x_j is the data from the jth pixel. The mean ($\bar{z}$), pedestal I_0, and peak (I_1) of the expression $I\left(z_j; \overline{A}, I_0, I_1, \bar{z}, \overline{\sigma}\right)$ are the fit variables.

Figure 14(a) is an example of the bunch distribution in CESR that was fit to the asymmetric Gaussian function with the mean sigma and asymmetry factor and (b) the residual from this fit is determined from equation 7.

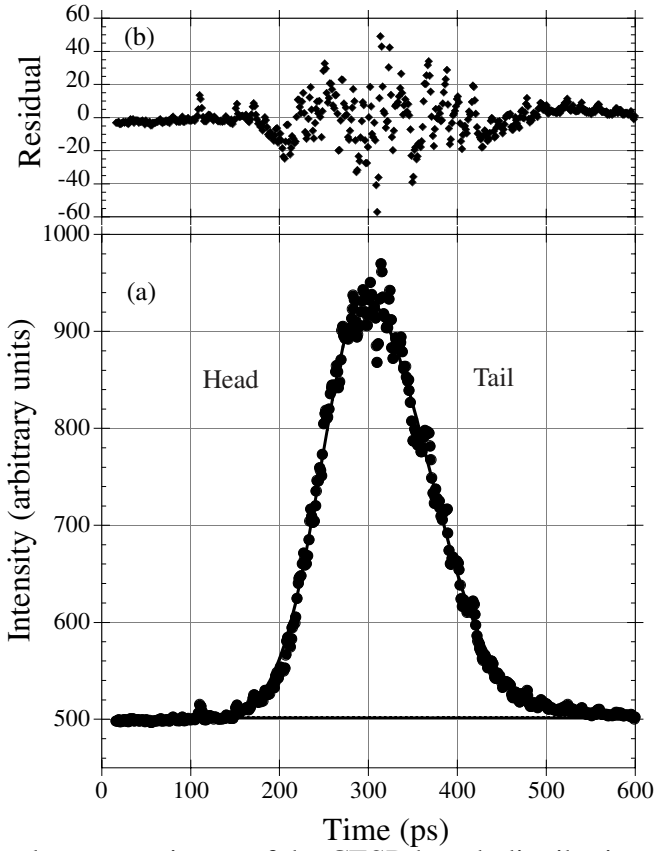

Figure 14. (a) A single streak camera picture of the CESR bunch distribution when fit to an asymmetric Gaussian function with the mean rms width and asymmetry factor from the experimental data set. This profile was measured with a single bunch of 30.7 mA. (b) The residual is the difference between the data and the fit.

The residuals from each experiment can also be summed to give the mean residual. The mean residual from an experimental data set is determined by summing up all the individual residuals in the data set. Because each profile has a different mean position, the residual from each profile is shifted so the mean of the asymmetric Gaussian is at the origin. The residual pixel intensity from each profile is then summed and averaged in two picosecond bins to remove the granularity of the calibration curve. The mean residual for the jth two picosecond bin is given by

$$\overline{R}_j = \frac{\sum_{i=1}^{m}\left(x_j - I\left(z_j;\overline{A},I_0,I_1,\overline{z},\overline{\sigma}\right)\right)}{m}$$

where $I\left(z_j;\overline{A},I_0,I_1,\overline{z},\overline{\sigma}\right)$ is the asymmetric Gaussian fit to the data when the mean rms width and asymmetry value are held constant and m is the number of pictures taken during the experiment. Figure 15 is an example of the average residual for the experiment when the current was 30.7 mA.

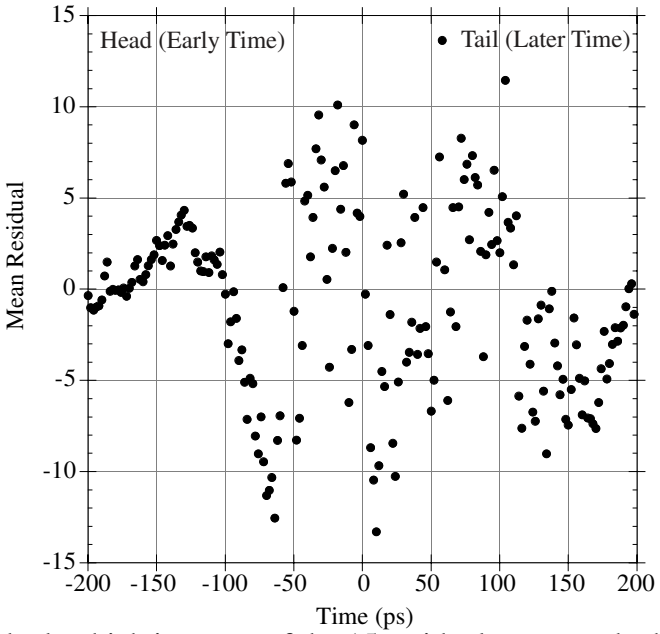

Figure 15. The mean residual, which is a sum of the 15 residuals, summed when the mean of the distribution is shifted to the origin. The single bunch current during this measurement was 30.7 mA.

It should be noted that caution should be taken when dealing with residuals because an instability oscillates and if the camera's data taking is not correlated with this oscillation then the residual will wash out over many pictures.

Streak Camera Operations

(a) Time Calibration

The streak camera tube was calibrated at the Hamamatsu Corporation and the time calibration curve for the streak speed used in these measurements is shown in figure 16. The calibration data was fit to a polynomial curve that was used in the analysis of the data. Each profile is corrected for time width of each bin (pixel) and this is done by dividing the background subtracted intensity by the calibration curve. The image intensity j at time t_i is corrected by

$$\mathrm{Bin_j}(t_i) = \frac{\mathrm{Bin_j}(I) - I_0}{\mathrm{Calib}(I)}$$

where I_0 is the background determined from the fit to the data. The calibration curve $\mathrm{Calib}(I)$ and time t_i is given by

$$\mathrm{Calib}(I) = 1.3647 - 9.6146\mathrm{x}10^{-4} I + 6.9609\mathrm{x}10^{-7} I^2$$

$$t_i = \int \mathrm{Calib}(I)\mathrm{dI} = 1.3647\mathrm{I} - 4.8073\mathrm{x}10^{-4}\mathrm{I}^2 + 2.3203x10^{-7} I^3$$

for pixel I.

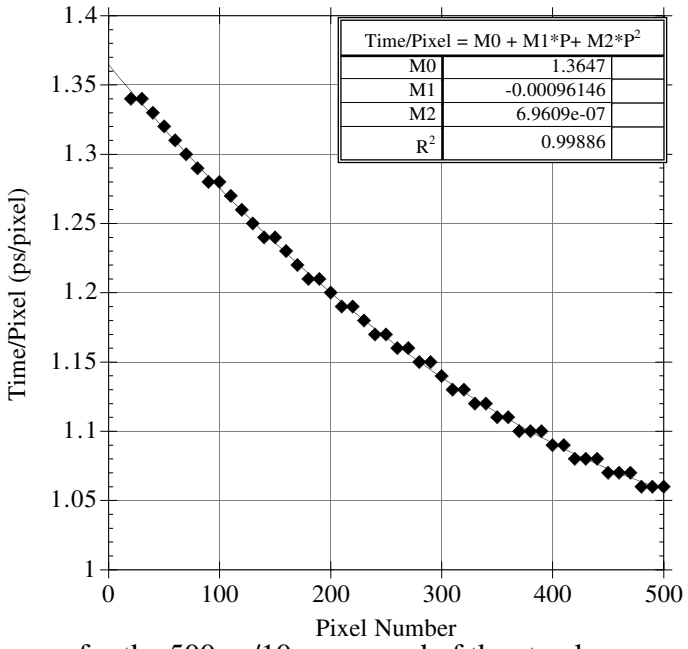

Figure 16. The linearity curve for the 500 ps/10 mm speed of the streak camera provided by the Hamamatsu Corporation. The data is fit to a second order polynomial which is used as the time calibration of the streak camera profiles.

The steak camera's read out monitor had a 600 ps window to observe the bunch distribution. This 600 ps window allowed the time calibration of the camera to be confirmed by measuring the beam location on the streak camera and varying the trigger signal. The trigger signal for the streak camera had a fine delay of 82 ps and adjusting the trigger in 82 ps steps, for a total of seven trigger settings, allowed the time calibration to be measured. In actuality only six trigger settings were used because the image was not visible in the window for the seventh trigger setting. The measurement consisted of taking 15 streak camera pictures at each trigger time, for a total of 90 pictures, when the streak image was visible in the 600 ps window. The 90 pictures were taken under constant machine conditions to avoid any systematic error associated with unstable running. The 15 images from each trigger setting were fit to an asymmetric Gaussian function and the average of the 15 mean positions were calculated to determine the mean location of the bunch relative subsequent trigger settings. The time difference on the camera was then determined from the calibration curve (figure 16) and compared with the trigger delay. Two of the data sets, which are separated by five 82 ps (for a total of 410 ps) trigger settings, are plotted in figure 17. The mean difference measured by the streak camera between the two trigger settings is $\delta t = T_2 - T_1 = 419.9 \pm 11.2\, ps$ which is in agreement with the expected value.

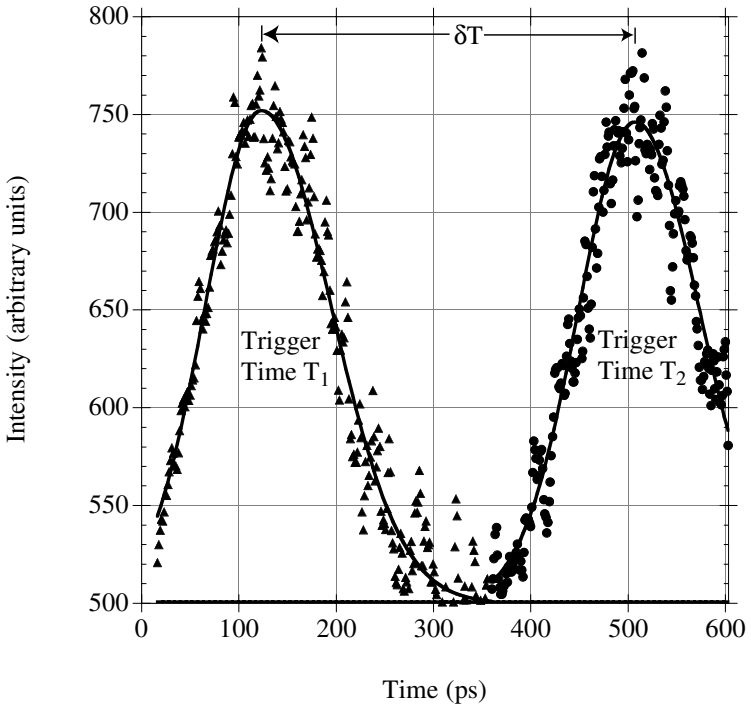

Figure 17. The sum of 15 streak camera pictures for two separate trigger settings, T_1 and T_2, where the trigger settings were separated by 410 ps.

(b) Resolution

The streak camera resolution at zero slit width has been measured for the two fastest streak speeds (60 ps/mm and 200 ps/mm) at the Stanford Linear Accelerator Center (SLAC) for the Stanford Linear Collider using a titanium sapphire 200 fs pulsed laser[7]. The bunch length at CESR is approximately 3 times larger than the SLAC damping ring so a slower streak speed was used, 500 ps/mm, and the resolution of the camera was not measured using the pulsed laser at the slower streak speed. Instead, the resolution can be determined by using the data from the faster streak speed with the calibration curve from the slower streak speed to fit the data. This is a viable alternative because the zero slit resolution is approximately 1% of the total streak time and the slit size determines the rest of the resolution component. Therefore the resolution at the 500 ps/10 mm speed uses the following methodology: 1) The zero slit resolution is assumed to be 1% of the full streak speed, which means 6.03 ps[9]. 2) The functionality of slit size can be determined by measuring the bunch length as a function of slit size for the faster streak speed laser pulses. By this methodology, the bunch length as a function of slit for the 500 ps/10 mm streak speed is shown in figure 18 (a). Most of the measurements were conducted on CESR with a slit width of 200 mm. The resolution correction is determined from figure 18 (b).

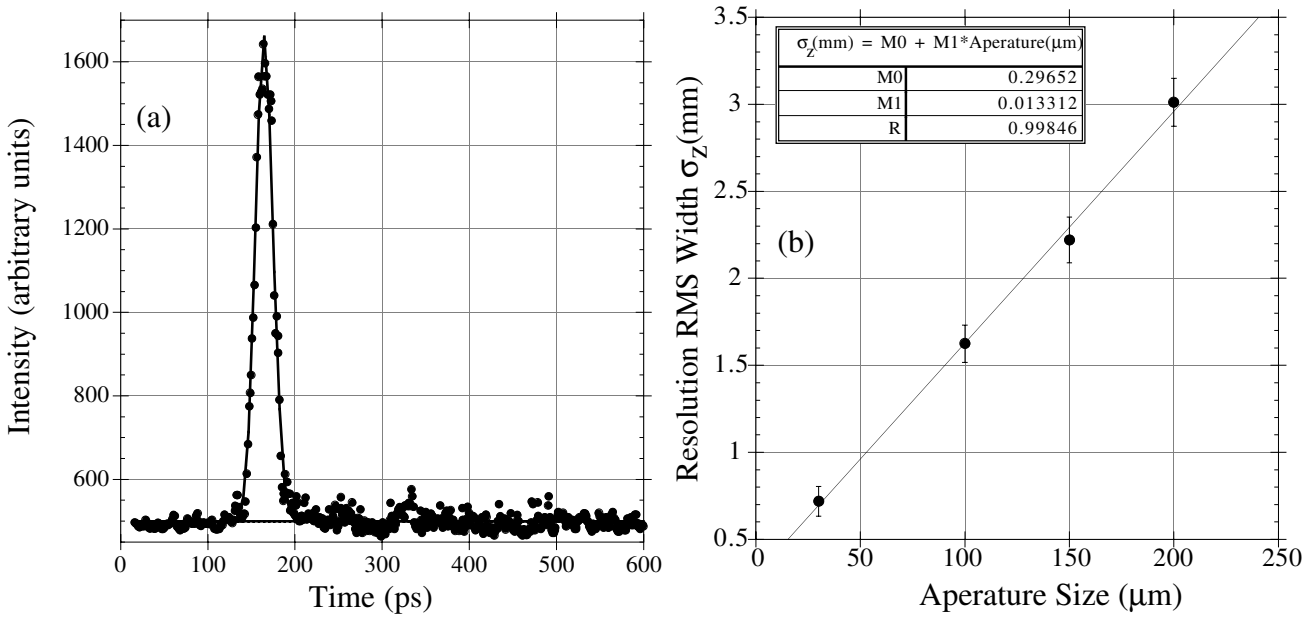

Figure 18. (a) A single picture of the longitudinal distribution of the pulsed laser with the streak camera when the slit of the camera is set to $200\mu m$. The fit of the pulse determines the resolution of the camera at this slit size. In this particular picture the rms pulse width is $\sigma_t = 10.06\text{ps}$. (b) The resolution of the streak camera as a function of slit size for the 500 ps/10 mm streak speed.

(c) Systematic Errors Associated with the Streak Camera

A description of the known systematic errors associated with this streak camera, such as chromatic and space charge effects, are described in detail elsewhere[7]. A systematic error associated with the camera's sensitivity was discovered while analyzing the time calibration data. A test of the streak camera's sensitivity (due to either the photocathode or multichannel plate) is to measure the sensitivity of these devices by summing up all of the pictures taken during the time calibration measurement. Each pixel was summed in the following manner:

$$P_{total}(i) = \sum_{j=1}^{n} P_j(i)$$

where $P_{total}(i)$ is the total intensity for pixel i for n pictures and $P_j(i)$ is the intensity for pixel i for a picture j. $P_{total}(i)$ is plotted for all 90 pictures taken during the linearity measurement and it is evident that pixels between number 195 and 278 have a reduced sensitivity to the input signal. Correcting pixels 195 to 278 is done by fitting the summed image to a third order polynomial and adjusting each pixel by the residual shown in figure 19 (a). Before the sensitivity correction the bunch length and mean position on the streak camera were highly correlated and this correlation was eliminated by enhancing pixels 195 to 278 by the amount shown in figure 19 (b).

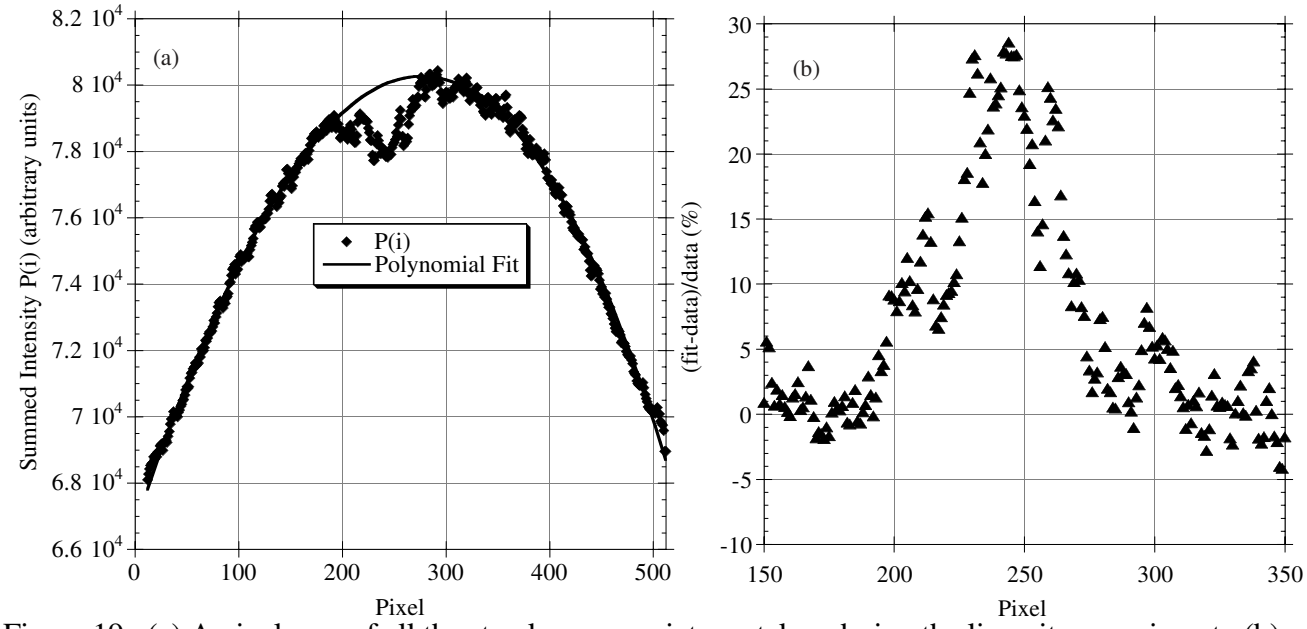

Figure 19. (a) A pixel sum of all the streak camera pictures taken during the linearity experiment. (b) The residual between the polynomial fit and the data. The residual shown here is used to correct the sensitivity. The pixels between 195 and 278 are enhanced by the amount shown in figure (b).

CESR Single Bunch Longitudinal Dynamics

The following measurements were made on CESR with the streak camera, 1) The bunch length at low current, 2) The bunch length as a function of current with the wiggler magnets closed and open, 3) The bunch length as a function of RF accelerating voltage at low and high current.

(I) Low Current Bunch Length

The longitudinal distribution at low current is valuable due to minimized collective effects and this gives the opportunity to compare the CESR model with the time calibration of the streak camera. The low current bunch distribution for electrons were measured by taking approximately 15 pictures with a single bunch in CESR. Measurements were made on the electrons when the wiggler magnets were open and closed and the RF accelerating voltage was $V_{RF} = 6.87 \pm 0.01 MV$. Since the measurements were made on electrons there is a pretzel orbit change between the wiggler open and closed conditions. The light intensity was low for these measurements and this required that the streak camera slit be set to $300 \mu m$ instead of $200 \mu m$ (the normal setting) for greater light acceptance. The longitudinal profiles were fit to an asymmetric Gaussian function with a constant background. A single snap shot of the bunch distribution with the wiggler open and closed is shown in figures 20 (a) and (b).

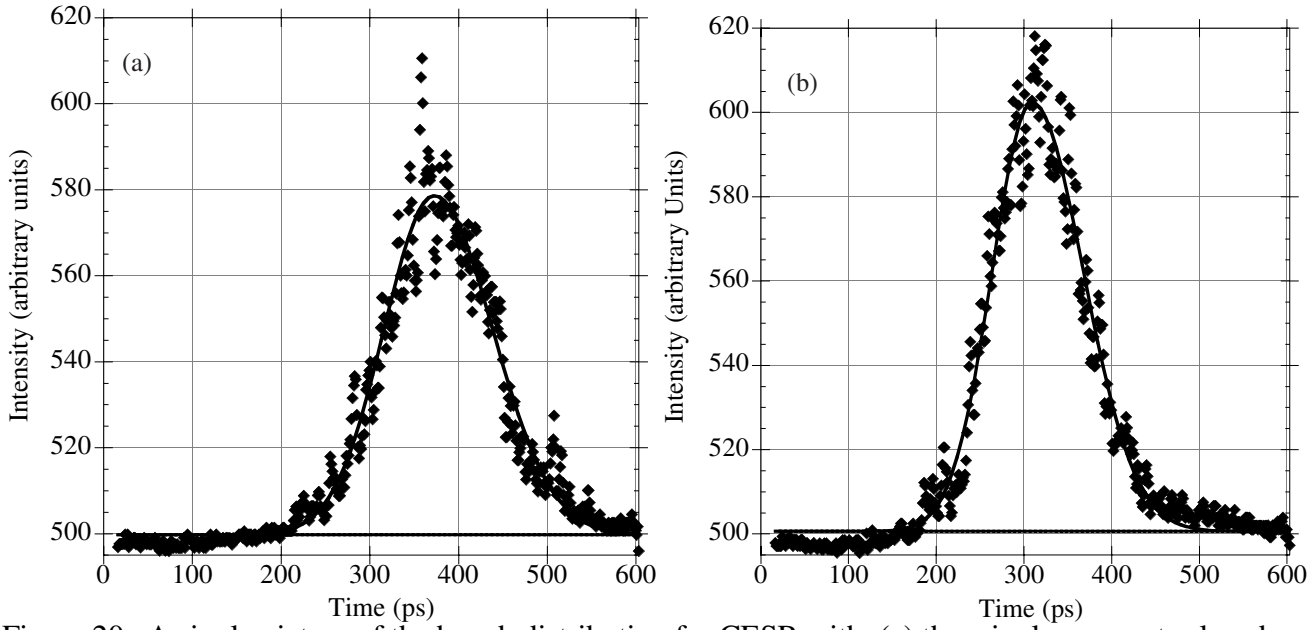

Figure 20. A single picture of the bunch distribution for CESR with: (a) the wiggler magnets closed, a current of 1.4 mA, and RF accelerating voltage at 6.87 MV. (b) The wiggler magnets open, a current 1.4 mA, and RF accelerating voltage of 6.87 MV.

The mean bunch length and asymmetry factor for the two cases is shown in table 6.

	RMS σ_z(mm)	Asymmetry Factor	Distribution Peak	CESR model σ_z(mm)
Wigglers Closed	17.89 ± 0.35	-0.020 ± 0.022	70.8 ± 2.7	17.39
Wigglers Open	15.91 ± 0.12	-0.0024 ± 0.029	106.7 ± 3.6	15.65

Table 6. The CESR low current bunch length results with wiggler magnets open and closed.

The results at low current provide the following information:

1) The mean peak of the longitudinal distribution differs between the open and closed wiggler magnet cases by 33%. This difference in distribution peaks can be attributed to the acceptance of synchrotron light optics. The electron beam's pretzel orbit changes when the wiggler magnets are turned on and this changes the acceptance of the synchrotron light. The light intensity was observed to go down when the wiggler magnets were closed and that corresponds to a lower peak in the distribution for the wiggler closed case.

2) There is a curvature to the streak camera background level. This curvature is evident at low light intensity (i.e. low current) and effects the asymmetry and bunch length measurements. This curvature is a result of running the camera at the high trigger repetition rate of $500 Hz$. The high trigger rate does not allow the CCD camera to completely refresh between pictures and this adds curvature to the background distribution in a location where the previous image was located on the CCD camera. To improve the fits to the distribution with the curved background, the following third order polynomial background fit is added

$$I(z) = I_0 + I_2 z + I_3 z^2 + I_4 z^3 + I_1 \exp\left\{-\frac{1}{2}\left(\frac{(z-\bar{z})}{(1+sgn(z-\bar{z})A)\sigma}\right)^2\right\}.$$

When fitting with the above function the bunch length is reduced by 5.5% with the wiggler magnets closed and by 3.7% with the wiggler magnets open. Figures 21 (a) and (b) are examples of fits with the curved background.

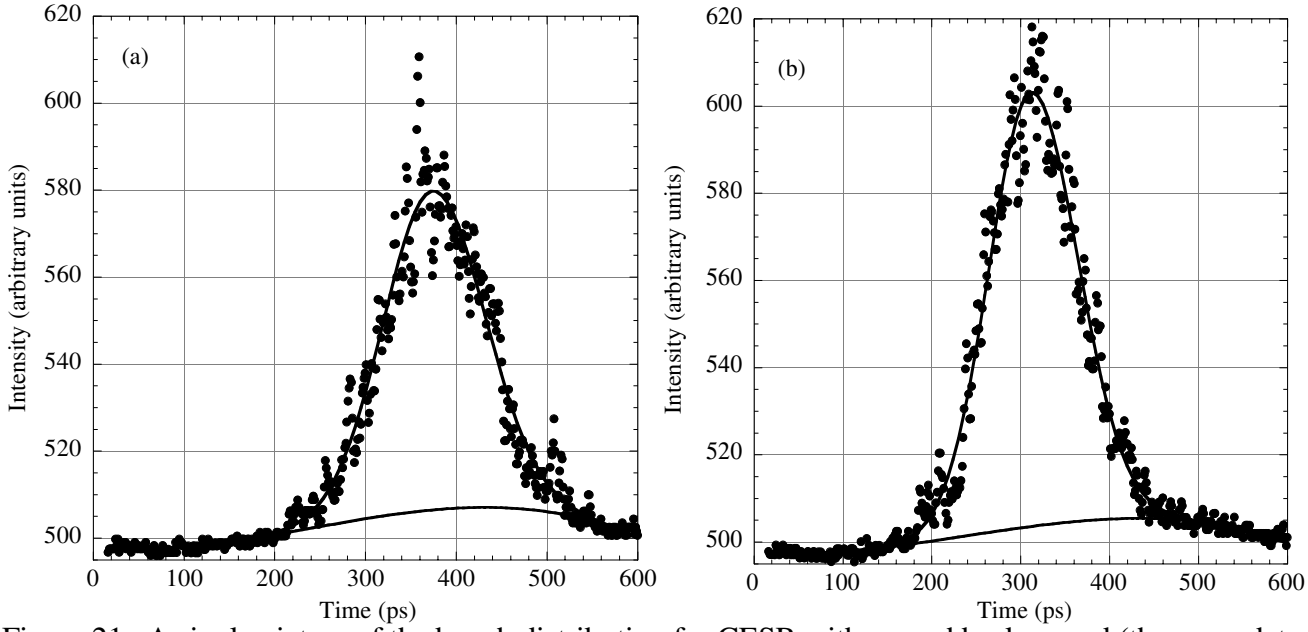

Figure 21. A single picture of the bunch distribution for CESR with curved background (the same data shown in figure 20) with (a) the wiggler magnets closed, and (b) the wiggler magnets open.

The χ^2 divided by the number of degrees of freedom is slightly reduced for the curved background fits but it adds another systematic error because it correlates the present picture of the bunch distribution with the previous picture of the bunch distribution. It should be noted, as the current increases this background curvature goes away and as a result, the bunch length and asymmetry factor with a flat background and curved background fit are identical.

3) A comparison of the streak camera measurements to the CESR model is made in table 6. Ignoring collective effects of the beam, the theoretical bunch length is 3.3% smaller than the measured bunch length when the wiggler magnets are closed and 2.1% smaller than the measured bunch length when the wiggler magnets are open. This difference between the measured bunch length and CESR model is possibly due to an incorrect calibration of the sweep voltage for the streak camera or a systematic shift in the RF voltage calibration. A 5% error in the RF voltage calibration would resolve the difference between the measured bunch length and the CESR model bunch length.

4) The residuals from the fit can be used to determine if there is any bunch distribution motion. Figures 22 (a) and (b) are pictures of the difference between a single picture of the bunch distribution and the average bunch distribution when the wiggler magnets open and closed.

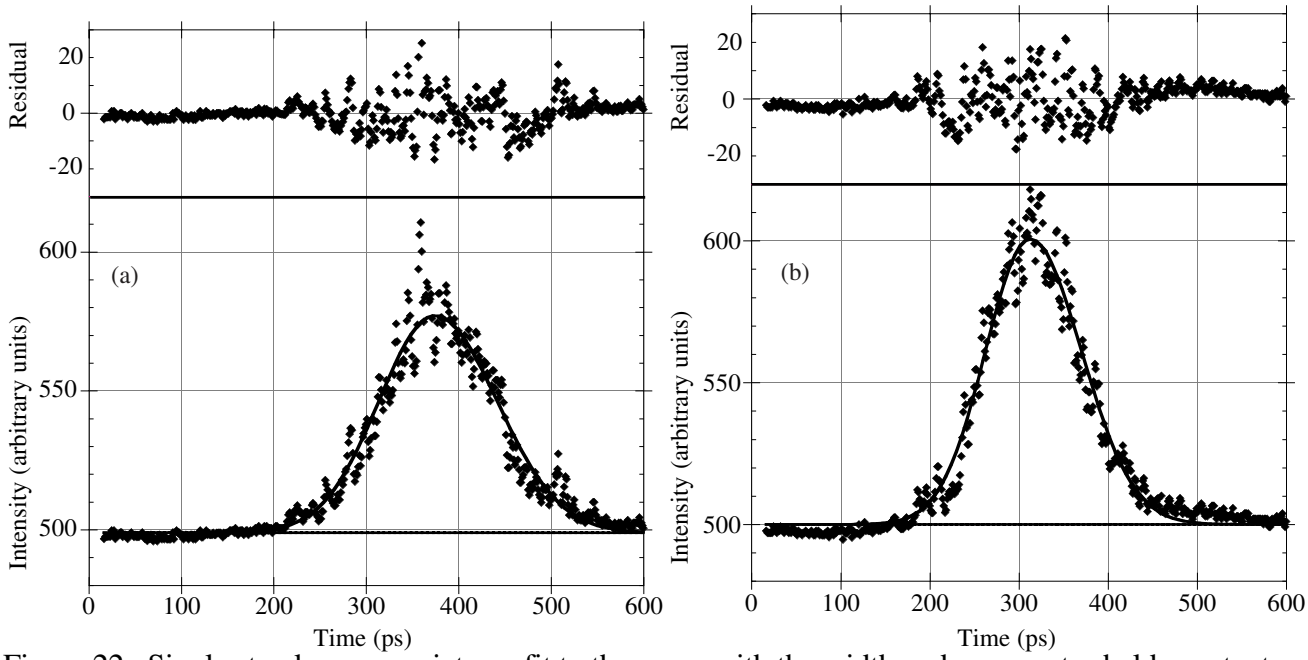

Figure 22. Single streak camera pictures fit to the mean with the width and asymmetry held constant. The residual from the fit is plotted above the distribution for the case when the wiggler magnets are (a) closed and (b) open.

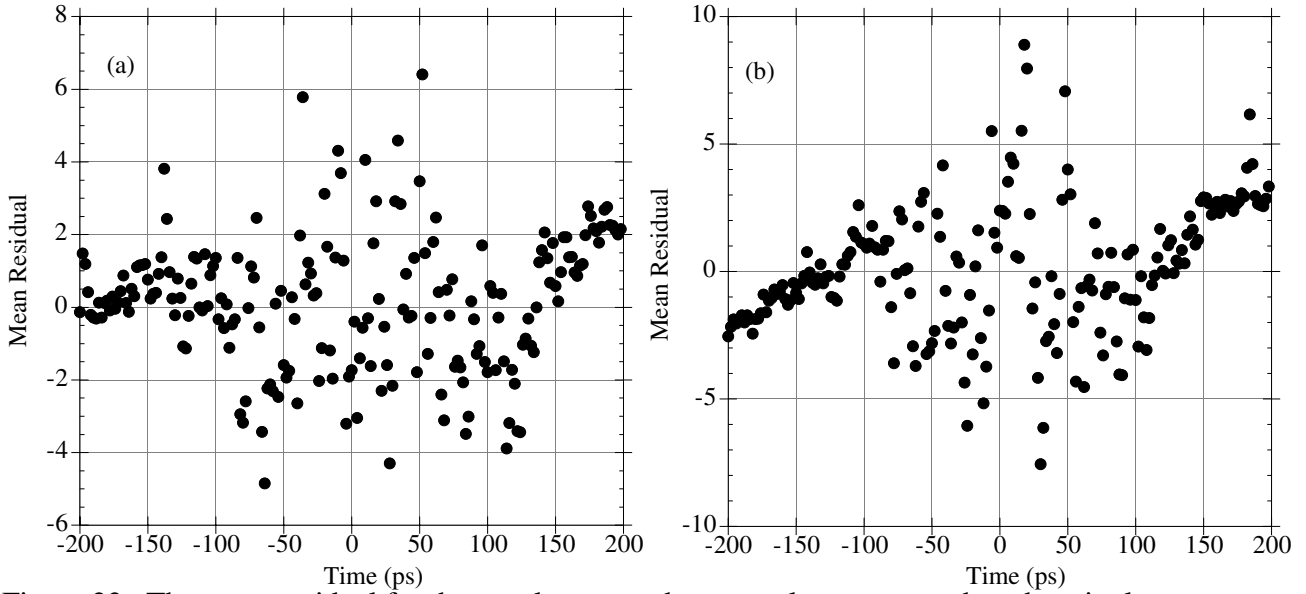

Figure 23. The mean residual for the streak camera data set at low current when the wiggler magnets were (a) closed and (b) open. The current and RF voltage were the same as stated in figure 20.

The sum of all the residuals is shown in Figures 23 (a) and (b). It is interesting to note that the background curvature is more evident in the case when the wiggler magnets were open and this could be due to high intensity levels. The deviation from the average distribution is not greater than 9% and this

can be attributed to the fluctuations in the light and noise in the camera. This deviation can be compared with higher current data. It should also be noted that no instability has been observed with the residual data.

(ii) Bunch length as a Function of Current

The electron bunch distribution was measured as a function of current with both wigglers open and closed. These measurements consisted of taking approximately 15 streak camera pictures at each current setting between the currents of 1 mA up to 35 mA with a single bunch in CESR RF setting is $V_{rf} = 6.87 \pm 0.01\text{MV}$. The light intensity increases as a function of current so neutral density filters were used to avoid saturation of the camera. The slit width of the streak camera was set to $200\mu m$ except at the lowest current setting when it was $300\mu m$. The profiles were fit to an asymmetric Gaussian function with a constant background and mean bunch length and asymmetry are computed. The mean length and asymmetry were used to compute the average residual from the set of data. A plot of the bunch length and asymmetry factor as a function of current with the wigglers open and closed is shown in Figures 24 (a) and (b).

There are several noteworthy features of the experimental data. 1) The bunch length increases linearly with current, denoted by the fit to the data in figure 24 (a), when the wigglers are open but when the wigglers are closed the bunch length remains fairly constant until approximately 10 mA, when the length increases dramatically. There is a 12% growth in the bunch length between the currents of 1 to 30 mA. This bunch lengthening is due to potential well distortion and the CESR vacuum chamber impedance can be determined from this data.

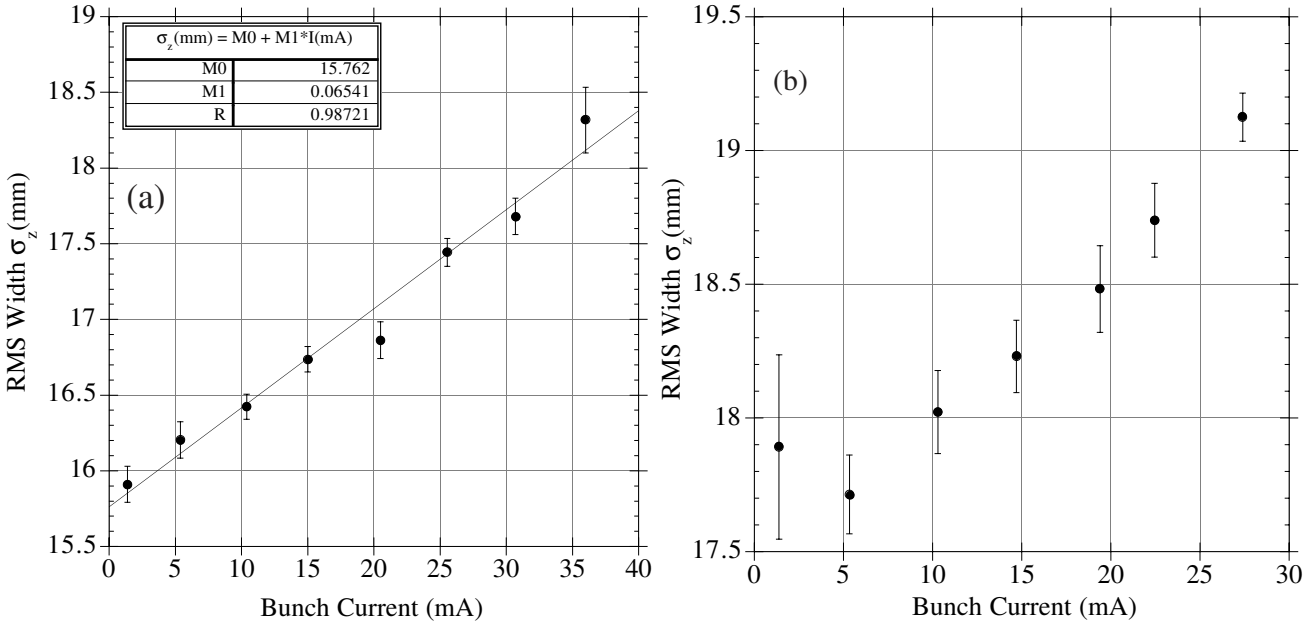

Figure 24. The bunch length in CESR as a function of current when the wiggler magnets are:(a) open and (b) closed.

2) The asymmetry factor (shown in figures 25 (a) and (b)), which measures the departure from a Gaussian distribution increases in both cases as a function of current. The asymmetry factor when the wigglers are open or closed is linear with current. The growth rate for the asymmetry factor in both cases are approximately the same.

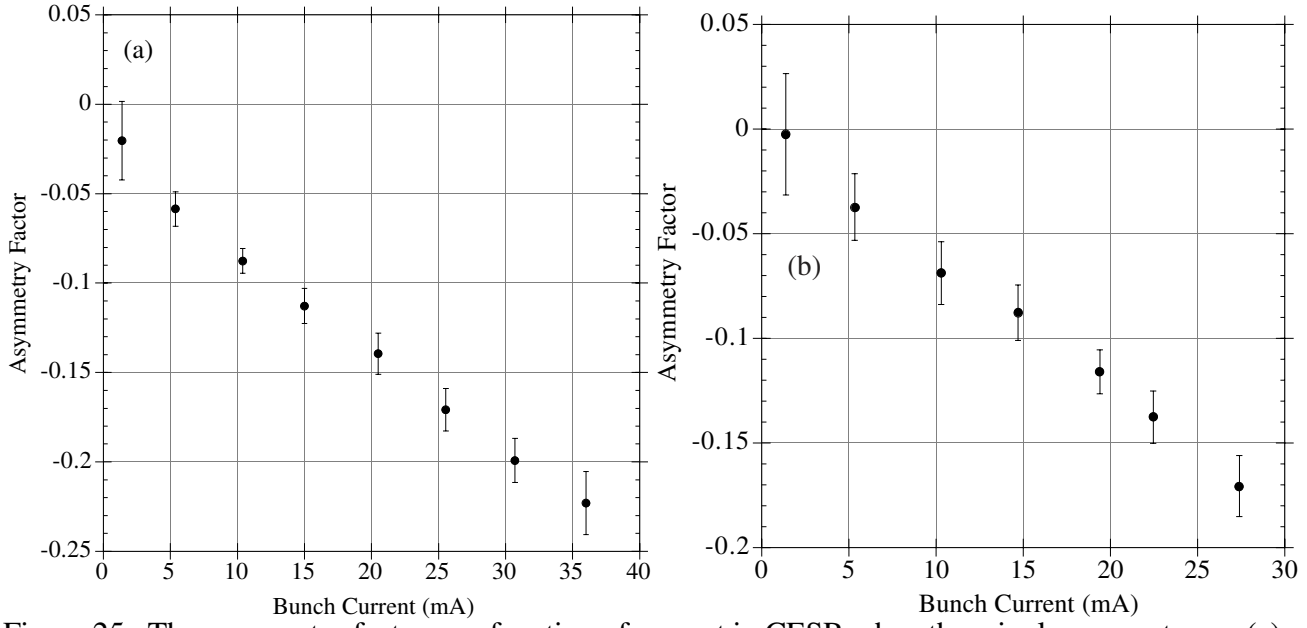

Figure 25. The asymmetry factor as a function of current in CESR when the wiggler magnets are: (a) open (b) closed